

## Liquid-vapor interface of an ionic fluid

B. Groh,<sup>1</sup> R. Evans,<sup>1,2</sup> and S. Dietrich<sup>1</sup>

<sup>1</sup>*Fachbereich Physik, Bergische Universität Wuppertal, D-42097 Wuppertal, Federal Republic of Germany*

<sup>2</sup>*H.H. Wills Physics Laboratory, University of Bristol, Bristol BS8 1TL, United Kingdom*

(Received 30 October 1997)

We investigate the liquid-vapor interface of the restricted primitive model (RPM) for an ionic fluid using a density-functional approximation based on correlation functions of the homogeneous fluid as obtained from the mean-spherical approximation. The ionic interfacial density profiles, which for the RPM are identical for both species, have a shape similar to those of simple atomic fluids in that the decay towards the bulk values is more rapid on the vapor side than on the liquid side. This is the opposite asymmetry of the decay to that found in earlier calculations for the RPM based on a square-gradient theory. The width of the interface is, for a wide range of temperatures, approximately four times the second moment correlation length of the liquid phase. We discuss the magnitude and temperature dependence of the surface tension and argue that for temperatures near the triple point the ratio of the dimensionless surface tension and critical temperature is much smaller for the RPM than for simple atomic fluids. [S1063-651X(98)13106-9]

PACS number(s): 68.10.-m, 61.20.Qg

### I. INTRODUCTION

In this paper we develop a density-functional theory (DFT) for the properties of the liquid-vapor interface of the simplest model of an ionic fluid, namely, the restricted primitive model (RPM) in which the ions are modeled by equisized hard spheres of equal and opposite charge. The RPM serves as a simple model for molten salts and electrolyte solutions. Indeed the measured partial structure factors  $S_{ij}(k)$ , with  $i, j \in \{+, -\}$ , and the thermodynamic properties of several molten alkali halides near their melting points can be well described by the corresponding quantities of the RPM [1]. In recent years there has been a revival of interest in the properties of the RPM, stemming from efforts to understand the nature of criticality in ionic fluids [2–4]. For ionic systems one might suppose that the long-range Coulomb forces could give rise to critical exponents different from the Ising ones that are measured and calculated for atomic and molecular fluids. Some recent experiments on certain electrolytes revealed mean-field-like behavior or, in some cases, Ising critical regions that are several orders of magnitude smaller than in atomic fluids [4]. Since the three-dimensional RPM is known to exhibit phase separation into a dense, conducting ionic liquid and a very dilute vapor phase, which is also conducting, it is a natural choice for theoretical and simulation studies of phase coexistence and criticality. Although attempts to explain the experimental observations regarding criticality have so far been unconvincing [estimates of the Ginzburg temperatures for the RPM are similar to those for simple (atomic) fluids [5,6] and the latest Monte Carlo finite-size scaling study [7] gives results compatible with Ising behavior] this does not mean that the RPM does not warrant further attention. On the contrary, because it incorporates the key features of hard-core repulsion and Coulomb forces it remains the canonical, albeit overidealized, model for an ionic fluid.

Here we shift attention away from the bulk and focus on the inhomogeneous situation that arises at the planar interface between the coexisting liquid and vapor of the RPM.

We are interested in the ionic density profiles and the surface tension of such an interface, which can be viewed as a crude model for the corresponding liquid-vapor interface of a molten alkali halide. Compared with the well studied case of simple fluids, modeled by a Lennard-Jones potential [8], very little is known about the interface in the RPM. We are not aware of any corresponding simulation studies, although there is one early molecular-dynamics simulation [9] using the more realistic Born-Mayer-Huggins potential model for KCl.

Theoretical work was pioneered by Telo da Gama *et al.* [10], who used the gradient expansion developed in Ref. [11] to investigate the RPM interface. The special symmetry of the RPM implies that the density profile of the cations should be the same as that of the anions, i.e., there should be local electroneutrality  $\rho_+(z) = \rho_-(z)$  throughout the interface. For such a “symmetric” situation the gradient expansion of the free-energy functional involves only gradients of the total density profile  $\rho(z) = \rho_+(z) + \rho_-(z)$ ; the charge density profile  $q(z) = \rho_+(z) - \rho_-(z)$  vanishes identically. The coefficients in this expansion involve moments of the density-density bulk direct correlation function  $c_\rho^{(b)}(r; \rho)$ . If the expansion is truncated at the square gradient term, as is usual, the corresponding coefficient must be positive if the theory is to yield physical solutions. As was explained in Ref. [10], it is necessary to utilize a rather sophisticated, self-consistent theory of the bulk correlation functions, the generalized mean-spherical approximation (GMSA) [12], in order to obtain a positive coefficient. The ordinary mean-spherical approximation (MSA) [13,14], which is often successfully employed [1] in studies of the bulk RPM, is insufficient as it yields merely the hard-sphere (Percus-Yevick) result for  $c_\rho^{(b)}(r; \rho)$  which produces a *negative* coefficient of the square-gradient term. That one must supercede the MSA to obtain physical interfaces is, at first sight, quite surprising, given its success in bulk. One suspects that this is an artifact of the square-gradient approximation. Here we reinvestigate the liquid-vapor interface using an alternative DFT, which

does not utilize the gradient expansion and thereby avoids the need to employ the GMSA and the ensuing problems involved with extrapolation into the two-phase region [10]. Our approach, which is motivated by the MSA treatment of the bulk free energy, involves a local density approximation for the hard-sphere part of the functional and a nonlocal treatment of the remaining (Coulombic) contributions, which is obtained by approximating the inhomogeneous pair correlation functions by their homogeneous counterparts. It differs from other DFT approaches for ionic fluids [15–19] that have proved successful in the primitive model description of electrical double layers at charged hard walls. These theories treat the non-hard-sphere part of the functional by means of a second-order density expansion about the density of a reference fluid, usually taken to be the homogeneous bulk fluid far from the substrate. Although this is adequate for many purposes it is problematical when it comes to liquid-vapor interfaces or to the adsorption of thick (wetting) films, where *two* bulk phases are involved. Indeed, for the case of an atomic fluid the corresponding second-order expansion about a homogeneous reference density is known to fail to account for liquid-vapor coexistence and is inadequate for wetting problems [20]. We are not aware of attempts to use the approaches in Refs. [15–19] for the liquid-vapor interface. Nor are we aware of attempts to use integral-equation theories for that purpose, which have been rather popular in studies of the electrical double layer [21,19] but may be beset by similar problems.

The present approach does not suffer from these difficulties, i.e., the uniform limit of the free energy reduces to that of the MSA for any uniform density  $\rho_b$ . On the negative side this means that our theory for the interface is prone to the same deficiencies as the bulk MSA, namely, the failure to incorporate properly the effects of ion pairing, which are especially pronounced in the vapor, and the consequent poor estimate of the location of the critical point.

As well as providing a description of the liquid-vapor interface of a near-symmetric alkali halide, i.e., one where the ions have nearly the same diameter, the present theory may form the basis for a description of wetting phenomena in ionic fluids [22]. The situations one would like to consider are (i) the wetting of a substrate–alkali-halide-vapor interface by the molten salt and (ii) the wetting of the interface between a substrate and, say, the phase dilute in salt by the other, salt-rich, phase for an electrolyte that exhibits liquid-liquid phase separation such as those considered in Refs. [4] and [23]. Since it is well known that wetting properties depend sensitively on the range of the interaction potentials, one might ask if the long-range Coulomb interactions lead to qualitatively new features or if, due to screening, ionic fluids behave as one-component systems with short-range interactions, e.g., Yukawa fluids.

This paper is arranged as follows. In Sec. II we introduce the approximate DFT for our particular problem. Section III examines the free energy and the second moment correlation length that emerge for the *bulk* fluid, comparing and contrasting the results with those of other theories and with exact results for the limit  $\rho \rightarrow 0$ . In Sec. IV we describe the results for the density profile and surface tension of the liquid-vapor interface as a function of temperature. These are compared with those of the earlier square-gradient theory

[10] and with corresponding results for simple atomic fluids. We conclude in Sec. V with a summary and discussion of our results.

## II. DENSITY-FUNCTIONAL THEORY FOR IONIC FLUIDS

We study the simplest model for an ionic fluid, the so-called restricted primitive model, which consists of charged hard spheres with equal diameters  $a$  for both species. It can be considered as a model of a molten salt, but also of an electrolyte solution with the solvent treated as a dielectric continuum. The interaction potential is given by

$$w_{ij}(r) = w^{HS}(r) + w_{ij}^C(r) \quad (1)$$

where

$$w^{HS}(r) = \begin{cases} \infty, & r < a \\ 0, & r > a \end{cases} \quad (2)$$

and

$$w_{ij}^C(r) = \frac{e_i e_j}{\epsilon r} \Theta(r-a) \quad (3)$$

where  $r$  is the interparticle distance,  $\Theta$  is the Heaviside step function,  $i, j \in \{+, -\}$ ,  $e_+ = -e_- = e$  is the charge of the particles, and  $\epsilon$  is the dielectric constant of the solvent.

The grand-canonical density functional of an inhomogeneous fluid with number densities  $\rho_i(\mathbf{r})$  can be written as

$$\begin{aligned} \Omega[\{\rho_i(\mathbf{r})\}] &= \mathcal{F}_{HS}[\{\rho_i(\mathbf{r})\}] + \frac{1}{2} \sum_{i,j} \int d^3r \int d^3r' \rho_i(\mathbf{r}) \rho_j(\mathbf{r}') \\ &\times \int_0^1 d\alpha w_{ij}^C(r_{12}) g_{ij}(\mathbf{r}, \mathbf{r}', \{\rho_i(\mathbf{r})\}, \alpha) \\ &- \sum_i \int d^3r \mu_i \rho_i(\mathbf{r}). \end{aligned} \quad (4)$$

Here  $\mathcal{F}_{HS}$  is the free-energy functional of the corresponding hard-sphere reference fluid,  $\mathbf{r}_{12} = \mathbf{r} - \mathbf{r}'$ ,  $\mu_i$  is the chemical potential of species  $i$ , and  $g_{ij}$  denotes the pair distribution function of an inhomogeneous system with the density profiles  $\rho_i(\mathbf{r})$  and the interaction potential  $w^{HS}(r) + \alpha w_{ij}^C(r)$ . The integration over  $\alpha \in [0, 1]$  corresponds to a straight line in potential space leading from the hard-sphere reference potential  $w^{HS}$  to the full potential  $w_{ij}$ . For the present model this path corresponds to a charging process of the ionic liquid. Although Eq. (4) is formally exact [24], the pair distribution function is not known for the inhomogeneous system. We approximate  $g_{ij}$  by the corresponding function  $g_{ij}(\mathbf{r} - \mathbf{r}', \bar{\rho}, \alpha)$  of a homogeneous (bulk) liquid evaluated at an appropriate density  $\bar{\rho}$ , for which we choose the mean value of the total densities at the points  $\mathbf{r}$  and  $\mathbf{r}'$ :

$$\bar{\rho} = \bar{\rho}(\mathbf{r}, \mathbf{r}') = \frac{1}{2} \sum_i [\rho_i(\mathbf{r}) + \rho_i(\mathbf{r}')]. \quad (5)$$

A similar averaging was used in Ref. [25] in a DFT for a Lennard-Jones fluid in contact with a hard wall. However, in

that work the local densities were additionally averaged over spherical regions around  $\mathbf{r}$  and  $\mathbf{r}'$ , which is not necessary in the present case because there are no pronounced density oscillations at the liquid-vapor interface. Note that the bulk pair distribution function  $g_{ij}$  depends only on the total density  $\rho = \rho_+ + \rho_-$ , which follows from the requirement of electroneutrality,  $\rho_+ = \rho_-$ , in the bulk. [Strictly speaking,  $g_{ij}(\mathbf{r}-\mathbf{r}', \bar{\rho}, \alpha)$  is not defined for densities that lie within the two-phase coexistence region of the bulk phase diagram, but this problem does not arise for the approximate pair distribution functions we shall actually use in our calculations below.]

By writing  $g_{ij} = 1 + h_{ij}$  the pure Coulombic contribution to the functional

$$\mathcal{F}^C[\{\rho_i(\mathbf{r})\}] = \frac{1}{2} \sum_{i,j} \int d^3r d^3r' \rho_i(\mathbf{r}) \rho_j(\mathbf{r}') w_{ij}^C(r_{12}) \quad (6)$$

can be separated off. In the bulk, where  $\rho_+ = \rho_-$ ,  $\mathcal{F}^C$  vanishes. Similarly, due to the symmetry of the RPM under charge inversion, the density distributions that minimize Eq. (4) at the free liquid-vapor interface should exhibit local charge neutrality, i.e.,  $\rho_+(\mathbf{r}) = \rho_-(\mathbf{r}) = \frac{1}{2}\rho(\mathbf{r})$ . Moreover, the symmetry of the RPM implies that the total pair correlation functions  $h_{ij}$  must satisfy  $h_{++} = h_{--}$  and  $h_{+-} = h_{-+}$ , so that Eq. (4) reduces to a functional of the total density  $\rho(\mathbf{r})$ :

$$\begin{aligned} \Omega[\{\rho(\mathbf{r})\}] &= \mathcal{F}_{HS}[\{\rho(\mathbf{r})\}] + \frac{1}{2} \int d^3r d^3r' \rho(\mathbf{r}) \rho(\mathbf{r}') \\ &\times \int_0^1 d\alpha \frac{e^2}{\epsilon r_{12}} h_D(r_{12}, \bar{\rho}(\mathbf{r}, \mathbf{r}'), \alpha) \\ &- \mu \int d^3r \rho(\mathbf{r}), \end{aligned} \quad (7)$$

with the difference function  $h_D = (h_{++} - h_{+-})/2$  and  $\mu = (\mu_+ + \mu_-)/2$ . The hard-sphere contribution is treated in a local density approximation

$$\begin{aligned} \mathcal{F}_{HS}[\{\rho(\mathbf{r})\}] &= \frac{1}{\beta} \int d^3r [\rho(\mathbf{r}) \{\ln[\rho(\mathbf{r}) \lambda^3] - 1\} \\ &+ \beta f_{CS}(\rho(\mathbf{r}))]. \end{aligned} \quad (8)$$

$\lambda$  is the thermal de Broglie wavelength and  $f_{CS}$  is the non-ideal gas part of the free-energy density of the bulk hard-sphere fluid given by the accurate Carnahan-Starling approximation [26]

$$f_{CS}(\rho) = \frac{\rho}{\beta} \frac{4\eta - 3\eta^2}{(1-\eta)^2}, \quad (9)$$

with the packing fraction  $\eta = (\pi/6)\rho a^3$ . Clearly the approximation given by Eq. (8) does not take into account the short-range correlations associated with the packing constraints that give rise to the oscillatory density profiles encountered for fluids at walls. Nor will it account for the weak oscillations that are predicted for low temperatures on the liquid side of the liquid-vapor density profile in both simple [27]

and ionic [28] fluids. A nonlocal treatment of  $\mathcal{F}_{HS}$  would be required to describe such oscillatory behavior.

We employ the bulk correlation function  $h_D$  given by the analytically solvable MSA [13,14], which provides a reasonable description of the bulk structure and thermodynamics of the RPM. Henderson and Smith [29] have derived an explicit expression for  $h_D$ :

$$\begin{aligned} h_D(r, \rho, T) &= -\frac{\beta e^2}{\epsilon r} \frac{1}{(1+a\Gamma)^2} \\ &\times \sum_{n=1}^{[r/a]} e^{-(r-na)\Gamma} \frac{[(r-na)\Gamma]^n}{(n-1)!} \\ &\times [j_{n-2}((r-na)\Gamma) - j_{n-1}((r-na)\Gamma)], \end{aligned} \quad (10)$$

where  $[r/a]$  is the largest integer smaller than  $r/a$ ,  $j_n$  denotes the spherical Bessel function of order  $n$  and the inverse length  $\Gamma$  is given by  $\Gamma = (\sqrt{1+2\kappa a} - 1)/2a$  with the inverse Debye screening length  $\kappa = (4\pi\beta e^2 \rho / \epsilon)^{1/2}$ . Expression (10) is inconvenient for the numerical calculation of  $h_D$  at large  $r$  because in this case many terms have to be evaluated and rather large errors may occur due to partial cancellations of the terms. On the other hand, a very good approximation for  $h_D$  for large  $r$  can be obtained from the pole analysis of the Fourier transform  $h_D(k)$  as shown by Leote de Carvalho and Evans [28]. It provides the asymptotes of the form

$$h_D(r \rightarrow \infty, \rho, T) = \frac{A(\rho, T)}{r} \exp[-\alpha_0(\kappa)r]$$

for  $\kappa < \kappa_c = 1.228/a$  and

$$h_D(r, \rho, T) = \frac{B(\rho, T)}{r} \exp[-\alpha_0(\kappa)r] \cos[\alpha_1(\kappa)r + \theta(\kappa)]$$

for  $\kappa > \kappa_c$  with known functions  $A$ ,  $B$ ,  $\alpha_0$ ,  $\alpha_1$ , and  $\theta$ . Using these methods we have derived similar but slightly more complicated expressions for  $(\partial/\partial\rho)h_D$  and  $(\partial^2/\partial\rho^2)h_D$ , which are needed to compute the phase diagram and the correlation length (see Sec. III). These asymptotic approximations have been used in the numerical calculations for  $r/a > 12$ .

### III. BULK PHASE DIAGRAM AND CORRELATION LENGTH

For a constant density  $\rho(\mathbf{r}) = \rho$  the density functional yields a Helmholtz free-energy density

$$\frac{F(\rho)}{V} = \frac{\rho}{\beta} [\ln(\rho \lambda^3) - 1] + f_{CS}(\rho) + \frac{1}{2} \rho^2 w_0(\rho), \quad (11)$$

with

$$w_0(\rho) = \frac{e^2}{\epsilon} \int d^3r r^{-1} \int_0^1 d\alpha h_D(r, \rho, \alpha). \quad (12)$$

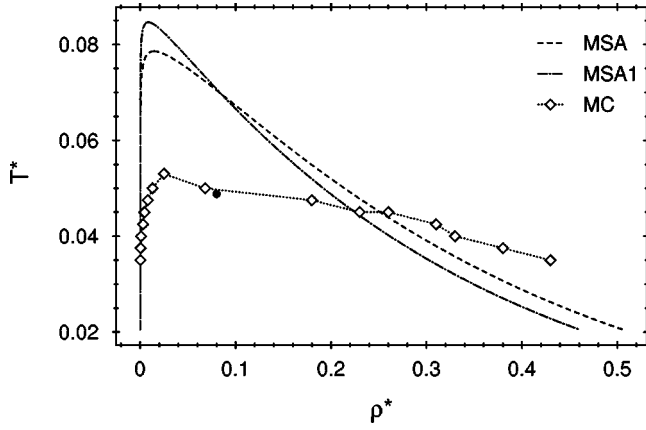


FIG. 1. Phase diagram of the restricted primitive model in the temperature-density plane as given by the MSA and MSA1 schemes discussed in the main text. The open symbols denote the results of Gibbs ensemble Monte Carlo simulations [32]. The solid circle denotes the most recent simulation estimate of the critical point [7]. The vapor-liquid-bcc-solid triple point is estimated to lie near  $T_r^* \approx 0.025$  and  $\rho_r^* \approx 0.5$  [33]. The dotted line connecting the Monte Carlo data is a guide to the eye.

Since  $h_D$  depends only on the dimensionless quantities  $\beta e^2/\epsilon a$  and  $r/a$ , the charging integration with  $e^2(\alpha) = \alpha e^2$  can be replaced by an integration over  $\beta$ :

$$w_0(\rho) = \frac{e^2}{\beta \epsilon} \int d^3r r^{-1} \int_0^\beta d\beta' h_D(r, \rho, \beta'). \quad (13)$$

This result demonstrates that the free energy given by Eqs. (11) and (12) is equal to that obtained by the so-called energy route starting from the MSA pair correlation function. Thus the bulk phase diagram is identical to the usual MSA phase diagram as discussed, e.g., in Refs. [30,31,10,28,5]. The explicit expression for  $w_0(\rho)$  is [14]

$$\frac{1}{2} \rho^2 w_0(\rho) = -\frac{1}{4\pi\beta a^3} \left( (\kappa a)^2 + 2\kappa a + \frac{2}{3} - \frac{2}{3} (1 + 2\kappa a)^{3/2} \right). \quad (14)$$

For the reasons discussed in Sec. IV below, we also consider the functional that arises when we refrain from the integration over  $\alpha$  and set  $\alpha=1$  instead, which amounts to replacing the excess free energy  $\mathcal{F}_{ex} = \mathcal{F} - \mathcal{F}_{HS}$  due to the Coulomb interactions by the corresponding internal energy  $U_{ex} = (\partial/\partial\beta)(\beta\mathcal{F}_{ex})$  [see Eq. (13)]. We call this approximation scheme MSA1. In this case Eq. (14) is replaced by

$$\frac{1}{2} \rho^2 w_0(\rho) = -\frac{1}{4\pi\beta a^3} [\kappa a + (\kappa a)^2 - \kappa a \sqrt{1 + 2\kappa a}]. \quad (15)$$

Note that, in contrast to Eq. (14), this expression does not reduce to the exact Debye-Hückel result  $\frac{1}{2} \rho^2 w_0(\rho) = -\kappa^3/12\pi\beta$  in the low-density ( $\kappa \rightarrow 0$ ) limit. However, it differs only by a factor of  $\frac{3}{2}$ .

The liquid-vapor phase coexistence curves, which follow from the free energy by the usual double tangent construction, are shown in Fig. 1 for the MSA and MSA1, together with the Gibbs ensemble Monte Carlo simulation results

[32,33]. The results are given in terms of the reduced density  $\rho^* = \rho a^3$  and the reduced temperature  $T^* = k_B T \epsilon a / e^2$ . The phase diagram of the RPM is characterized by small values of the reduced critical density and temperature (for comparison the Lennard-Jones fluid has  $T_c^* \approx 1.3$  and  $\rho_c^* \approx 0.3$  in Lennard-Jones reduced units) and by a strong asymmetry of the coexistence curve. At low temperatures the vapor phase becomes extremely dilute, e.g., at  $T^* = 0.04 \approx T_c^*/2$  one has  $\rho_v^* \approx 10^{-7}$  within the MSA. It is well known that the MSA overestimates the critical temperature and grossly underestimates the critical density. The cruder MSA1 predicts an even higher critical temperature (for the MSA  $T_c^* = 0.0786$ , and for the MSA1,  $T_c^* = 0.0846$ ) and smaller critical density (for the MSA,  $\rho_c^* = 0.0145$ , and for the MSA1  $\rho_c^* = 0.0086$ ). Simulation results for the coexistence curve have undergone substantial revision during recent years (see, e.g., Refs. [2,3]); the latest estimate of the critical point by Caillol *et al.* [7], using a mixed-field finite-size analysis of Monte Carlo data, gives  $T_c^* = 0.0488 \pm 0.0002$  and  $\rho_c^* = 0.080 \pm 0.005$ . Clearly quantitatively reliable results cannot be expected from either the MSA or MSA1. Both fail to take proper account of the effects of ion pairing, which is known to be very strong in the RPM at low densities and is believed to influence strongly the location of the critical point [30,2,3]. Since the differences between the coexistence curves obtained from the MSA and MSA1 are relatively minor, we do not expect to introduce significant additional errors by using the MSA1. We note that the main contributions to the integration over  $\alpha$  in Eq. (12) stem from the region near  $\alpha=1$ .

The chemical potential  $\mu_0$  at coexistence is, for a given temperature,

$$\mu_0 = \left. \frac{\partial F(\rho)}{\partial \rho} \right|_{\rho_l} = \left. \frac{\partial F(\rho)}{\partial \rho} \right|_{\rho_v}, \quad (16)$$

where  $\rho_l$  and  $\rho_v$  are the densities of liquid and vapor, respectively. Knowledge of  $\mu_0(T)$  is a prerequisite for the subsequent analysis of the liquid-vapor interface.

We now turn attention to the bulk correlation length that follows from the present theory. As we shall see in Sec. IV, the width of the interface is governed by the correlation length of the bulk liquid. Every density-functional ansatz defines a direct correlation function via twofold functional differentiation of the intrinsic Helmholtz free-energy functional  $\mathcal{F}[\{\rho_i(\mathbf{r})\}]$  with respect to density [24]:

$$c_{ij}(\mathbf{r}, \mathbf{r}', \{\rho_i(\mathbf{r})\}) = -\beta \frac{\delta^2 \mathcal{F}[\{\rho_i(\mathbf{r})\}]}{\delta \rho_i(\mathbf{r}) \delta \rho_j(\mathbf{r}')} + \frac{\delta_{ij} \delta(\mathbf{r} - \mathbf{r}')}{\rho_i(\mathbf{r})}. \quad (17)$$

From the bulk limit of this function a pair distribution function  $h_{ij}$  can then be obtained via the Ornstein-Zernike equation. The results will be different from the  $h_{ij}$  used for the construction of the functional, in our case those of the MSA. This is an important advantage of the density-functional approach. We require the correlation function for fluctuations of the total density  $h_\rho^{(b)} = (h_{++} + h_{+-})/2$  to exhibit the conventional Ornstein-Zernike behavior, i.e.,  $h_\rho^{(b)}$  should become long ranged near the critical point, with an exponential decay described by a diverging correlation length. Such a

behavior reflects the net interparticle interaction that is necessary to obtain liquid-vapor coexistence. However, as remarked in the Introduction, the original MSA result for  $h_\rho^{(b)}$  is simply that of hard spheres (in the Percus-Yevick approximation), so there is no manifestation of attraction in this particular combination of the correlation functions. We define the second-moment correlation length  $\xi$  for fluctuations of the total density by the expansion of the structure factor

$$S(k, \rho) = 1 + \rho h_\rho^{(b)}(k, \rho) = S(0, \rho) / (1 + \xi^2 k^2 + \dots), \quad (18)$$

where  $k$  is the wave number. This correlation length can be obtained rather easily if one again assumes  $\rho_+(\mathbf{r}) = \rho_-(\mathbf{r}) = \frac{1}{2}\rho(\mathbf{r})$  and considers  $\mathcal{F} = \Omega + \mu \int d^3r \rho(\mathbf{r})$  [see Eq. (7)] as a functional of the total density  $\rho(\mathbf{r})$ . Using the bulk limit  $c_\rho^{(b)}$  of the function

$$c_\rho(\mathbf{r}, \mathbf{r}', \{\rho(\mathbf{r})\}) = -\beta \frac{\delta^2 \mathcal{F}[\{\rho(\mathbf{r})\}]}{\delta \rho(\mathbf{r}) \delta \rho(\mathbf{r}')} + \frac{\delta(\mathbf{r} - \mathbf{r}')}{\rho(\mathbf{r})}, \quad (19)$$

$\xi$  is given by

$$\xi^2 = \frac{1}{6} \frac{\int d^3r r^2 c_\rho^{(b)}(r, \rho)}{1/\rho - \int d^3r c_\rho^{(b)}(r, \rho)}, \quad (20)$$

which follows straightforwardly from the definition given by Eq. (18) and the Ornstein-Zernike equation  $h_\rho^{(b)}(k, \rho) = c_\rho^{(b)}(k, \rho) / [1 - \rho c_\rho^{(b)}(k, \rho)]$ . Within the MSA1 one finds

$$\begin{aligned} \beta^{-1} c_\rho^{(b)}(r, \rho) = & -\delta(\mathbf{r}) \frac{\partial^2}{\partial \rho^2} f_{CS}(\rho) - \frac{e^2}{\epsilon r} \left( h_D(r, \rho) \right. \\ & \left. + \rho \frac{\partial}{\partial \rho} h_D(r, \rho) + \frac{1}{4} \rho^2 \frac{\partial^2}{\partial \rho^2} h_D(r, \rho) \right) - \delta(\mathbf{r}) \\ & \times \int d^3r' \frac{e^2}{\epsilon r'} \left( \rho \frac{\partial}{\partial \rho} h_D(r', \rho) \right. \\ & \left. + \frac{1}{4} \rho^2 \frac{\partial^2}{\partial \rho^2} h_D(r', \rho) \right). \end{aligned} \quad (21)$$

Note that the equivalent result for a simple atomic fluid was derived in Ref. [34]. The resulting correlation lengths of the coexisting liquid and vapor phases are plotted in Fig. 2. In accordance with the mean-field character of the present approach they diverge near the critical point proportional to  $(T_c - T)^{1/2}$ .  $\xi$  also diverges upon approaching the spinodals, which are determined by  $\partial^2 F(\rho) / \partial \rho^2 = 0$  or, equivalently, by the vanishing of the denominator in Eq. (20). Upon lowering the temperature the correlation length in the liquid phase decreases to about one particle diameter, whereas that of the vapor phase increases again as a consequence of the reduced screening at very low densities.

It is instructive to examine the limiting behavior as  $\rho \rightarrow 0$ . The exact low-density behavior of the second moment correlation length is believed to be [35]

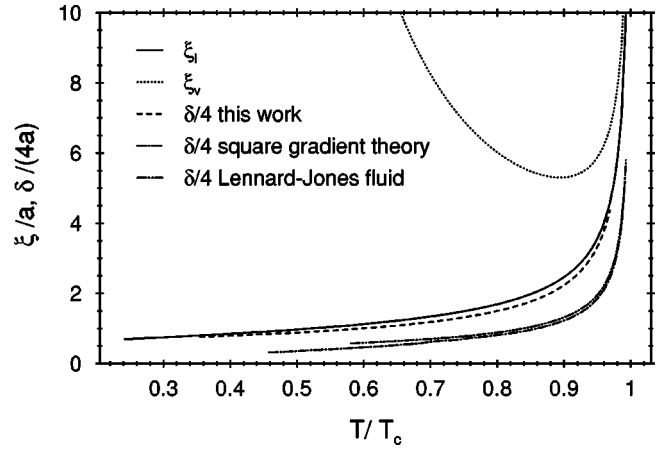


FIG. 2. Second moment correlation lengths  $\xi_v$  and  $\xi_l$  for density correlations in the vapor and liquid phases at two-phase coexistence obtained using the MSA1. Also shown is the width  $\delta$  [defined by Eq. (35)] of the liquid-vapor interface obtained from the present density-functional theory and from the square gradient theory of Ref. [10]. All lengths diverge at the critical temperature  $T_c$ . The vapor correlation length increases at low temperatures because of the reduced screening in the very dilute vapor phase. The interfacial width  $\delta$  is very close to  $4\xi_l$  over the whole temperature range. At the same reduced temperature the interfacial width predicted by the present theory is larger than that obtained from the square-gradient theory, which in turn is close to the result for a Lennard-Jones fluid as obtained from a DFT similar to the present one [39].

$$\xi = \frac{1}{4} \left( \frac{\beta e^2}{36\pi\epsilon\rho} \right)^{1/4} [1 + O(\rho^{1/2})], \quad (22)$$

a result that also follows from the hypernetted-chain approximation [36,35]. If one assumes that for low densities the MSA correlation function  $h_D$  tends to  $-(\beta e^2/\epsilon r)e^{-\kappa r}$ , all the algebra can be performed analytically and the MSA1 yields in leading order

$$\xi = \left( \frac{7}{192\pi} \frac{\kappa}{\rho} \right)^{1/2} = \frac{\sqrt{7}}{4} \left( \frac{\beta e^2}{36\pi\epsilon\rho} \right)^{1/4}, \quad (23)$$

which is in accordance with our numerical results. Thus, for  $\rho \rightarrow 0$  the MSA1 correlation length diverges with the correct power law, but the amplitude is too large by a factor of  $\sqrt{7}$ . We can also carry through the algebra using the original functional (7) (including the  $\alpha$  integration). In this case we obtain

$$\xi = \frac{\sqrt{14}}{4} \left( \frac{\beta e^2}{36\pi\epsilon\rho} \right)^{1/4} \quad (24)$$

for  $\rho \rightarrow 0$ . Once again the power law is correct, but the amplitude is again too large. These results suggest that the functionals capture the essential features of density-density correlations in the  $\rho \rightarrow 0$  limit. This is a nontrivial observation. Recall that the GMSA, which assumes a particular (single Yukawa) form for the non-Coulomb part of the direct correlation functions  $c_{ij}(r)$  and then enforces consistency among three routes to bulk thermodynamic functions, yields a finite value as  $\rho \rightarrow 0$  [35]. Thus our present MSA1 and MSA results, Eq. (23) and (24), improve upon the GMSA in the

low-density limit. Finally we should emphasize that the results described here refer to the second moment correlation length  $\xi$  as defined by Eqs. (18) or (20). The so-called true correlation length  $\xi_\infty$  that determines the ultimate exponential decay of the density-density correlation function  $h_\rho^{(b)}(r, \rho)$  is determined by the poles of the Fourier transform  $h_\rho^{(b)}(k, \rho)$  [28]. In general,  $\xi_\infty$  differs from  $\xi$ ; they become identical (within mean-field theory) in the vicinity of the critical point. Calculating the poles from the present DFT approach is not straightforward as the Fourier transform of Eq. (21) cannot be performed analytically, so we cannot easily compute  $\xi_\infty$ . However, we are able to compare our results for  $\xi$  with  $\xi_{\infty, GMSA}$  obtained in Ref. [28]. For subcritical liquidlike states that turn out to be relevant for the interface, the correlation lengths  $\xi_{MSA}$  and  $\xi_{MSA1}$  both differ by less than a factor of 2 from  $\xi_{\infty, GMSA}$ . In the very-low-density vapor phase the exact limiting behavior is  $\xi_\infty \approx 1/2\kappa$  [36,35], which diverges as  $(T/\rho)^{1/2}$  for  $\rho \rightarrow 0$ , i.e., faster than the second moment correlation length given by Eq. (22).

In summary, we conclude that the present density-functional theory provides a reasonable description of the long-wavelength (small  $k$ ) behavior of density-density correlations in the bulk RPM. This is a necessary prerequisite for a reliable treatment of the liquid-vapor interface.

#### IV. LIQUID-VAPOR INTERFACE

##### A. Density profiles

The average density profile of the liquid-vapor interface varies only in the direction normal to the interface, which we take as the  $z$  direction. In the following we assume that the bulk liquid density  $\rho_l$  is obtained for  $z \rightarrow -\infty$  and the bulk vapor density  $\rho_v$  for  $z \rightarrow \infty$ . The application of the density-functional theory outlined in Sec. II to this situation allows one to carry out the lateral integrations in Eq. (7) yielding the following grand-canonical functional per surface area  $A$  for the total density  $\rho(z) = 2\rho_-(z) = 2\rho_+(z)$ :

$$\begin{aligned} \frac{1}{A} \Omega[\{\rho(z)\}] &= \frac{1}{A} \mathcal{F}_{HS}[\{\rho(z)\}] + \frac{1}{2} \int dz dz' \rho(z) \rho(z') \\ &\quad \times w(z-z', \bar{\rho}(z, z')) - \mu_0 \int dz \rho(z), \end{aligned} \quad (25)$$

with

$$w(z_{12}, \rho) = \frac{2\pi e^2}{\epsilon} \int_{|z_{12}|}^{\infty} dr \int_0^1 d\alpha h_D(r, \rho, \alpha). \quad (26)$$

For densities not too large the function  $h_D$  exhibits its slowest decay as a function of  $r$  [lowest value of  $\alpha_0(\kappa)$ , the imaginary part of the leading pole] for small values of the charge, i.e., for small  $\alpha$  [see Fig. 4(b) in Ref. [28]]. Therefore, in contrast to the bulk free energy, the large distance behavior of  $w(z_{12}, \rho)$  is dominated by the contributions from small  $\alpha$ . In this region the correlation function is expected to take on the Debye-Hückel form

$$h_D(r, \rho, \alpha) \approx -\frac{\beta e^2}{\epsilon r} \alpha e^{-\kappa \sqrt{\alpha} r}, \quad (27)$$

which also follows from the small coupling expansion of the decay length and of the expression for the amplitude obtained from the pole analysis [28] mentioned in Sec. III. From Eqs. (26) and (27) one finds

$$\frac{\partial}{\partial z} w(z \rightarrow \infty, \rho) \approx -\frac{2\pi \beta e^4}{\epsilon^2 z} \int_0^1 d\alpha \alpha e^{-\kappa \sqrt{\alpha} z} \quad (28)$$

and hence

$$w(z \rightarrow \infty, \rho) \approx -\frac{6\pi \beta e^4}{\epsilon^2 \kappa^4 z^4}. \quad (29)$$

Thus  $w$ , which corresponds to the effective interaction between two fluid layers a distance  $z$  apart, is predicted to decay algebraically with the same exponent as for a Lennard-Jones fluid, where the interatomic potential decays as  $r^{-6}$ . This unexpected result implies an algebraic decay for the density profiles too. More specifically one would expect  $d\rho/dz \sim -|z|^{-4}$  as  $z \rightarrow \pm\infty$ . This behavior can be traced back to the fact that within the MSA density-functional theory the bulk direct correlation function  $c_\rho^{(b)}(r, \rho)$ , which is given by Eq. (21) with  $h_D(r, \rho)$  replaced by  $\int_0^1 d\alpha h_D(r, \rho, \alpha)$ , also decays algebraically. Using an argument similar to the one above one finds  $c_\rho^{(b)}(r, \rho) \sim r^{-6}$  as  $r \rightarrow \infty$ , which is the same as for a Lennard-Jones fluid. This would in turn imply that  $h_\rho^{(b)}(r, \rho)$  as obtained from  $c_\rho^{(b)}(r, \rho)$  via the Ornstein-Zernike equation should also decay as  $r^{-6}$ . In other words, the theory generates effective potentials for density-density correlations that mimic those of genuine dispersion forces. While this observation is certainly intriguing it is likely to be an artifact of the present MSA scheme. The bulk pair correlation function  $h_\rho^{(b)}(r, \rho)$  should decay exponentially for the RPM [36,28]. Moreover, general arguments for the decay of density profiles near walls [27,28,37] show that the ultimate decay of  $\rho(z)$  should mimic that of  $h_\rho^{(b)}$ . For example,  $\rho_l - \rho(z)$  should decay as  $\exp(z/\xi_\infty)$  as  $z \rightarrow -\infty$ , where  $\xi_\infty$  is the true correlation length of the bulk liquid. If, on the other hand, we ignore the  $\alpha$  integration and set  $\alpha = 1$  (see also the discussion in Sec. III), then  $-\partial w(z, \rho)/\partial z \sim h_D(z, \rho)$  and there is no longer an algebraic decay of the direct correlation function and of the profile. Henceforward we describe results based on both MSA and MSA1.

By functional differentiation of Eq. (25) one derives the Euler-Lagrange equation

$$\ln \rho(z) \lambda^3 + f'_{CS}(\rho(z)) = \mu_0 - p(z), \quad (30)$$

with

$$\begin{aligned} p(z) &= \int dz' \rho(z') \left[ w(z-z', \bar{\rho}(z, z')) \right. \\ &\quad \left. + \frac{1}{2} \rho(z) w'(z-z', \bar{\rho}(z, z')) \right]. \end{aligned} \quad (31)$$

(The primes on  $f_{CS}$  and  $w$  denote derivatives with respect to the density.) In contrast to similar theories for Lennard-Jones [38] or dipolar [39] fluids the kernel in Eq. (31) depends on

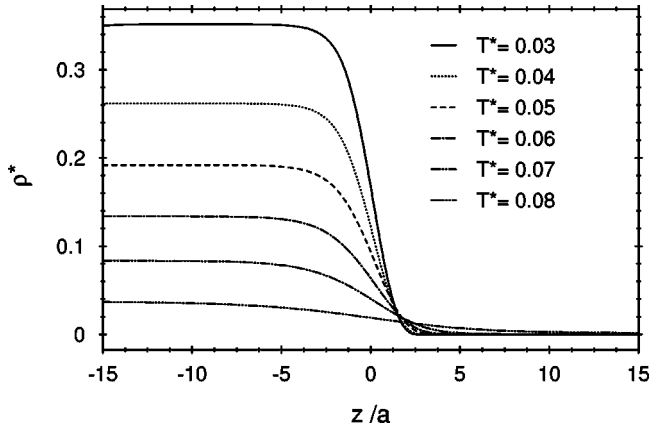


FIG. 3. Total density profile of the liquid-vapor interface of the RPM at different temperatures, as obtained from MSA1.

$z$  and  $z'$  separately due to the density dependence of the approximated pair distribution function. However, in the present case one can still show that if a profile  $\rho(z)$  solves Eq. (30) any shifted profile  $\rho(z-z_0)$  will be a solution as well because the position of the interface is not fixed by the boundary conditions. In order to select a unique profile we have imposed the additional requirement  $\rho(z=0) = (\rho_l - \rho_v)/2$  and have shifted the profiles accordingly during the numerical solution.

Equation (30) was solved using the usual Picard iteration scheme. In each iteration ( $n$ ) the function  $p(z)$  is calculated from the density profile  $\rho_{(n)}(z)$  in the region  $z \in [-L/2, L/2]$  and a new  $\rho_{new}(z)$  is obtained by numerical inversion of Eq. (30) for each value of  $z$ . In order to achieve convergence the profile for the next iteration is calculated according to the mixing rule

$$\rho_{(n+1)} = \omega \rho_{new} + (1 - \omega) \rho_{(n)}, \quad (32)$$

where typically  $\omega = 0.2$ . The process is repeated until  $\max_z |\rho_{(n+1)}(z) - \rho_{(n)}(z)|$  is smaller than a prescribed accuracy. Since the functions  $w(z_{12}, \rho)$  and  $w'(z_{12}, \rho)$  have discontinuous derivatives at  $z_{12} = \pm a$  the integration in Eq. (31) is divided into the three subintervals  $[-L/2, z-a]$ ,  $[z-a, z+a]$ , and  $[z+a, L/2]$ . The Milne rule, which effectively interpolates the integrand piecewise by third-order polynomials, is used for all integrations. Asymptotic contributions to  $p(z)$  from the regions  $|z'| > L/2$  are calculated by replacing  $\rho(z')$  by the bulk limits  $\rho(z' < -L/2) = \rho_l$  and  $\rho(z' > L/2) = \rho_v$  and integrating numerically with  $w(|z-z'| > 20a) = 0$ .

The functions  $w$  and  $w'$  are given by integrals over the functions  $h_D$  and  $h'_D$  whose evaluation already requires significant numerical efforts. Since  $w(z_{12}, \rho)$  and  $w'(z_{12}, \rho)$  have to be evaluated many times during the iteration scheme the algorithm can be accelerated considerably by using two-dimensional spline interpolations for these functions, which require their evaluation only at, e.g.,  $100 \times 100$  grid points before the main algorithm starts.

In Fig. 3 we plot the density profiles obtained from the MSA1 for a series of different temperatures. Upon increasing the temperature towards the critical point ( $T_c^* = 0.08465$ ) the interface broadens and the density difference  $\rho_l - \rho_v$  be-

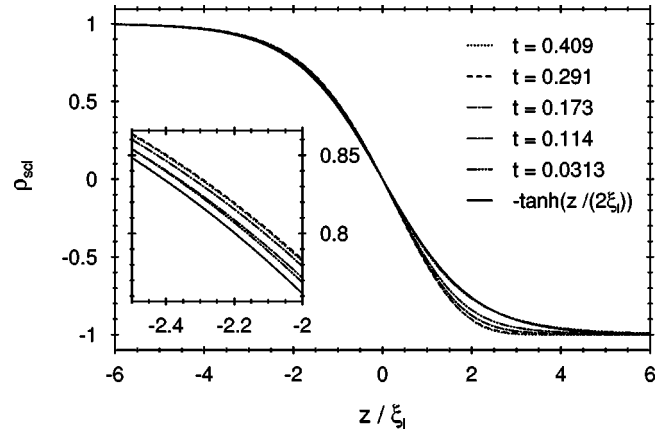


FIG. 4. Density profiles, as obtained from MSA1, plotted in scaled form [see Eq. (33)] as a function of  $z/\xi_l$ . The parameter  $t = 1 - T/T_c$  measures the deviation from the critical temperature. For  $t \rightarrow 0$  the scaled profiles approach the universal scaling function  $-\tanh(z/2\xi_l)$ .

tween the phases decreases. These obvious features can be incorporated by introducing a scaling function  $\rho_{scl}(z/\xi, T)$  with  $\rho_{scl}(\pm\infty, T) = \mp 1$ :

$$\rho(z, T) = \frac{1}{2}(\rho_l + \rho_v) + \frac{1}{2}(\rho_l - \rho_v) \rho_{scl}(z/\xi, T). \quad (33)$$

For  $T \rightarrow T_c$  the scaling function should reduce to a universal function of the single variable  $z/\xi$ , which, within mean-field theory, is given by

$$\rho_{scl}(z/\xi, T \rightarrow T_c) = -\tanh \frac{z}{2\xi}. \quad (34)$$

Such a plot is given in Fig. 4 using the second-moment correlation length  $\xi_l(T)$  for the bulk liquid phase, obtained from Eqs. (20) and (21). This demonstrates that the scaling behavior remains valid even relatively far outside the critical region. In order to make a comparison with the behavior of simple atomic fluids we present in Fig. 5 the density profiles of a Lennard-Jones fluid scaled in the same manner. These

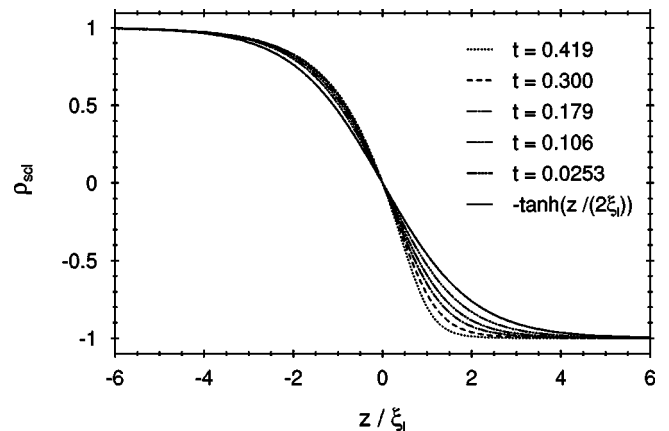


FIG. 5. Same plot as Fig. 4 but for a Lennard-Jones fluid. The results were obtained using the density-functional theory of Frod and Dietrich [39]. Note that the approach to the scaling limit is slower and the profiles are more asymmetric than for the ionic fluid.

results have been obtained using the density-functional ansatz of Frodl and Dietrich [39]. At low temperatures the profiles of the ionic fluid deviate weakly from antisymmetry, approaching the bulk limit faster on the vapor side than on the liquid side. The same trend can be observed in the Lennard-Jones system, where it is even more pronounced: Compare profiles corresponding to the same reduced temperature  $t = 1 - T/T_c$ . In the case of a Lennard-Jones fluid the deviation from antisymmetry is attributed [40] to the fact that  $\xi_v < \xi_l$  at low temperatures. The situation is different for the ionic case where, away from  $T_c$ ,  $\xi_v \gg \xi_l$  (see Fig. 2). This would imply that within a square-gradient theory there should be a *slower* decay of the profiles on the *vapor* side. The results of Ref. [10] are in accordance with this expectation. However, compared to the square-gradient theory, our present nonlocal theory clearly predicts the opposite asymmetry: The decay on the vapor side is *faster* than that on the liquid side, although  $\xi_v \gg \xi_l$ . In order to understand these features it is important to distinguish between the intermediate range decay that is apparent from Figs. 3–5 and the ultimate asymptotic decay into the bulk. As mentioned previously, for the ionic fluid the ultimate decay should be exponential with a decay length equal to the true correlation length  $\xi_\infty$  of the bulk. We attempted to analyze the numerical results for the tails of our profiles, but this is rather difficult because the variations are very small. When curves of the form  $C \exp(-|z|/\xi)$  or  $(C/z) \exp(-|z|/\xi)$  are fitted to the tails of the MSA1 profiles one finds larger values for  $\xi$  on the vapor side, as expected, but the actual values depend very strongly on the  $z$  interval used for the fitting. Finally, we note that the density profiles in a Lennard-Jones fluid approach, as a function of temperature, the universal scaling function monotonically from below on the vapor side and from above on the liquid side (see Fig. 5). On the other hand, in the ionic fluid the density profile on the vapor side is below the universal profile at low temperature but is above it for large  $z$  close and  $T$  to  $T_c$  (see Fig. 4 for  $t = 1 - T/T_c = 0.0313$ ). We interpret this as a consequence of the facts that  $\xi_v > \xi_l$  and that the vapor becomes more important near  $T_c$  due to its increasing density. At the same reduced temperature the scaled interfacial profiles in a Lennard-Jones fluid are steeper than those of the ionic fluid.

We define the interfacial width  $\delta$  as

$$\delta = -(\rho_l - \rho_v) \left( \frac{d\rho}{dz} \Big|_{z=0} \right)^{-1}. \quad (35)$$

For the tanh profile in Eq. (34) one has  $\delta = 4\xi$ , so that in the critical region  $\delta/4$  should diverge in the same way as the correlation length. Remarkably, Fig. 2 shows that at *all* temperatures this width is determined by the *liquid* correlation length  $\xi_l$ . At  $T^* = 0.03$ , which is a little higher than the estimated triple point temperature [33],  $\delta/a \approx 3.0$ . This value is slightly higher than the estimates of the equivalent ratio for simple atomic fluids near their triple points [8]. Also shown in Fig. 2 are the results of Ref. [10], which exhibit a similar variation with  $T$ , but at low  $T$  the widths are about a factor of 2 smaller. The ‘‘10–90’’ interfacial thickness used in Ref. [10] is defined as the distance over which the total density changes from  $\rho_v + 0.9(\rho_l - \rho_v)$  to  $\rho_v + 0.1(\rho_l - \rho_v)$ . For the tanh profile it gives a width that is larger by a factor

$\operatorname{arctanh}(0.8) = 1.0986$  than the quantity  $\delta$  defined in Eq. (35). The data taken from Ref. [10] have been divided by this factor. For the actual profiles shown in Fig. 3 the two definitions for the width yield values that differ by about 10% too.

The density profiles obtained from the MSA (including the  $\alpha$  integration) are, for a given value of  $t = 1 - T/T_c$ , similar to those obtained from the MSA1. When plotted in terms of scaled variables [Eq. (33)], the profiles from the two theories can hardly be distinguished on the scale of Fig. 4. Moreover, identifying the ultimate algebraic decay from the numerical results for the tails of the profiles was not feasible. The interfacial widths  $\delta$  calculated from the MSA profiles are close to  $4\xi_l$ , with  $\xi_l$  obtained within the MSA approach. These widths are in turn close to those from the MSA1, provided we make a comparison at the same value of  $t$ .

## B. Surface tension

In this subsection we present results of calculations of the liquid-vapor surface tension  $\gamma$ . First we derive an expression for  $\gamma$  in terms of the density profile  $\rho(z)$ , which is convenient for numerical work. Since it is necessary to cut off the system at  $z = \pm L/2$ , this generates artificial fluid-vacuum surface tensions  $\gamma_{l,vac}$  and  $\gamma_{v,vac}$ , which must be subtracted in order to obtain the liquid-vapor surface tension. Therefore,  $\gamma$  is given by

$$\gamma = \lim_{L \rightarrow \infty} \left[ \frac{\Omega(L)}{A} - \frac{\Omega_{bulk}}{A} \right] - \gamma_{l,vac} - \gamma_{v,vac}, \quad (36)$$

where  $\Omega(L)$  is the grand-canonical functional evaluated for a finite system of size  $L$ . It is convenient to express the bulk free energy [Eq. (11)] as a double integral over  $z$  and  $z'$  analogous to Eq. (25). A straightforward calculation yields

$$\int_0^{L/2} dz \int_0^{L/2} dz' w(z-z', \rho) = \frac{L}{2} w_0(\rho) - 2 \int_0^{L/2} dz t(z, \rho) \quad (37)$$

with  $t(z, \rho) = \int_z^\infty dy w(y, \rho)$  and, from Eqs. (13) and (26),

$$w_0(\rho) = 2 \int_0^\infty dy w(y, \rho) = 2t(0, \rho). \quad (38)$$

The surface tensions with the vacuum follow from assuming constant density profiles  $\rho(z) = \rho_b$ , with  $b = v, l$ , which leads to (there are two equal interfaces)

$$\gamma_{b,vac} = \frac{1}{2} \lim_{L \rightarrow \infty} \frac{1}{2} \rho_b^2 \left[ \int_{-L/2}^{L/2} dz \int_{-L/2}^{L/2} dz' w(z-z', \rho_b) - L w_0(\rho_b) \right]. \quad (39)$$

Using Eq. (37) and the symmetry  $w(-y) = w(y)$  gives



$$\begin{aligned}
\gamma_{b,vac} &= \frac{1}{2} \rho_b^2 \lim_{L \rightarrow \infty} \left[ \int_0^{L/2} dz \int_{-L/2}^0 dz' w(z-z', \rho_b) \right. \\
&\quad \left. - 2 \int_0^{L/2} dz t(z, \rho_b) \right] \\
&= \frac{1}{2} \rho_b^2 \lim_{L \rightarrow \infty} \left[ \int_0^{L/2} dz [t(z, \rho_b) - t(L/2+z, \rho_b)] \right. \\
&\quad \left. - 2 \int_0^{L/2} dz t(z, \rho_b) \right] \\
&= -\frac{1}{2} \rho_b^2 \int_0^\infty dz t(z, \rho_b). \tag{40}
\end{aligned}$$

Thus the final expression for the surface tension follows by inserting Eqs. (11), (37), and (40) into Eq. (36):

$$\begin{aligned}
\gamma &= \int_{-\infty}^\infty dz [f_{HS}(\rho(z)) - f_{HS}(\rho_{SK}(z))] - \mu_0 \int_{-\infty}^\infty dz [\rho(z) \\
&\quad - \rho_{SK}(z)] + \frac{1}{2} \int_0^\infty dz \int_0^\infty dz' [\rho(z) \rho(z') w(z-z', \bar{\rho}(z, z')) \\
&\quad - \rho_v^2 w(z-z', \rho_v)] + \frac{1}{2} \int_{-\infty}^0 dz \int_{-\infty}^0 dz' [\rho(z) \rho(z') \\
&\quad \times w(z-z', \bar{\rho}(z, z')) - \rho_l^2 w(z-z', \rho_l)] \\
&\quad + \int_{-\infty}^0 dz \int_0^\infty dz' \rho(z) \rho(z') w(z-z', \bar{\rho}(z, z')) \\
&\quad - \frac{1}{2} \rho_v^2 \int_0^\infty dz t(z, \rho_v) - \frac{1}{2} \rho_l^2 \int_0^\infty dz t(z, \rho_l), \tag{41}
\end{aligned}$$

with the sharp-kink profile

$$\rho_{SK}(z) = \begin{cases} \rho_l, & z < 0 \\ \rho_v, & z > 0 \end{cases} \tag{42}$$

and  $f_{HS}(\rho) = (\rho/\beta) [\ln(\rho\lambda^3) - 1] + f_{CS}(\rho)$ . All integrals occurring in Eq. (41) are convergent.

Since the surface tension is the surface excess grand potential per unit area, an alternative starting point is the formula

$$\gamma = \int_{-\infty}^\infty dz [\omega(z) + p] \tag{43}$$

with the grand-canonical potential density

$$\begin{aligned}
\omega(z) &= f_{HS}(z) - \mu_0 \rho(z) + \frac{1}{2} \rho(z) \\
&\quad \times \int_{-\infty}^\infty dz' \rho(z') w(z-z', \bar{\rho}(z, z')) \tag{44}
\end{aligned}$$

and the vapor pressure

$$p = -f_{HS}(\rho_b) + \mu_0 \rho_b - \frac{1}{2} \rho_b^2 w_0(\rho_b), \quad b = l, v. \tag{45}$$

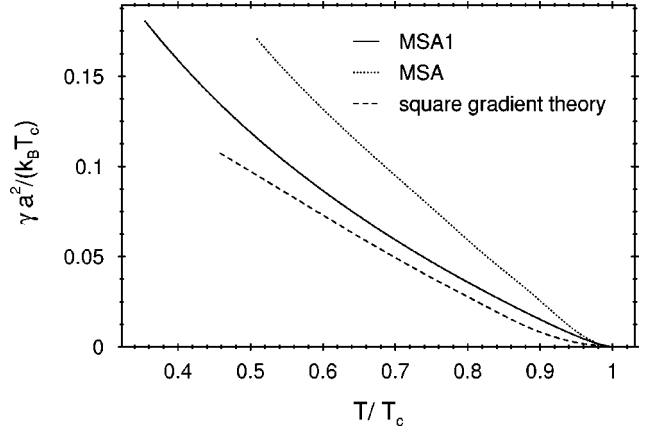


FIG. 6. Comparison of the liquid-vapor surface tension  $\gamma$  of the RPM as given by the present MSA and MSA1 theories and by the square gradient theory of Ref. [10]. The data have been reduced using the critical temperature  $T_c$  appropriate for each theory.

It is straightforward to show that Eq. (43) also leads to Eq. (41).

The surface tensions obtained from the MSA1 and MSA theories are displayed in Fig. 6 as a function of  $T/T_c$  and are compared with the results of the square-gradient theory [10]. Since the MSA1 has a higher critical temperature  $T_c$  than the MSA we plot the ratio  $\tilde{\gamma} = \gamma a^2 / k_B T_c$  rather than the reduced tension  $\gamma^* = \gamma \epsilon a^3 / e^2$ , which is displayed in Ref. [10]. The MSA results for  $\tilde{\gamma}$  are larger than the values predicted by MSA1, which in turn are larger than those obtained from the square-gradient theory, with the differences becoming larger at low temperatures. Near  $T_c$  all three theories yield the standard mean-field critical behavior, i.e.,  $\tilde{\gamma} \sim (1 - T/T_c)^{3/2}$ . At lower temperatures the square-gradient theory gives a nearly linear variation of  $\tilde{\gamma}$  with  $T/T_c$ , whereas in the MSA1 the  $(1 - T/T_c)^{3/2}$  behavior appears to persist further from  $T_c$ , which is consistent with the earlier observation that the density profiles follow the scaling behavior even for temperatures well removed from  $T_c$ .

The present MSA1 results predict  $\tilde{\gamma}(T/T_c = 0.6) \approx 0.09$ . This estimate should be contrasted with the corresponding result for a Lennard-Jones fluid where simulations and theories yield  $\tilde{\gamma}(T/T_c = 0.6) \approx 0.6$  [8]. The physical origin of such a large difference is not obvious and it is important to ask whether it is an artefact of the present approximations. Although our theories overestimate  $T_c$  they should make a compensating overestimation of the surface tension  $\gamma$ . It is conceivable that since MSA1 and MSA grossly underestimate, for a given value of  $T/T_c$ , the simulation results for the liquid densities at coexistence (see Fig. 1) they also underestimate the magnitude of  $\gamma$ . On the other hand, if one takes experimental data for the surface tension of molten alkali halides near the melting points and makes some reasonable estimates of the (average) diameter  $a$  the values of the resulting reduced tension  $\gamma^*$  [10] are similar to those obtained by extrapolating the present results to the appropriate reduced temperatures  $T^*$ . This would suggest that the present theories yield at least the correct order of magnitude for the surface tension  $\gamma$ .

## V. SUMMARY AND DISCUSSION

We have developed two, closely related, density-functional theories for the liquid-vapor interface of the RPM. Both the MSA and the MSA1 are based on approximating the inhomogeneous pair correlation function by that of a homogeneous bulk liquid at some mean density  $\bar{\rho}$ . The MSA1 involves an additional approximation, i.e., the integration over the coupling constant (charge) is ignored. The results that have emerged from this analysis can be summarized as follows.

(i) The MSA and MSA1 yield similar bulk phase diagrams, with the latter overestimating the critical temperature  $T_c$  and underestimating the critical density  $\rho_c$  to a further extent than the MSA (Fig. 1).

(ii) The two theories yield similar second moment correlation lengths for the density-density correlations in the bulk fluid (Fig. 2). They exhibit the correct power-law dependences in the low-density limit but overestimate their numerical prefactors [Eqs. (22)–(24)].

(iii) When suitably scaled to take into account the differences in the bulk phase diagram the total density profiles are similar in both theories. Both predict that for low temperatures and on intermediate length scales the profile approaches its bulk limits faster on the vapor side than on the liquid side (Figs. 3 and 4). This is opposite to what is found in the square-gradient theory of Ref. [10]. However, the ultimate decay into bulk should be determined by the bulk correlation length, which is larger on the vapor side.

(iv) The interfacial width  $\delta$ , defined by Eq. (35), is close to four times the *liquid* correlation length over the whole temperature range. It is larger but has a similar variation compared to that of a simple liquid with temperature (Fig. 2).

(v) For  $T \rightarrow T_c$  the density profiles approach a universal scaling form. In contrast to simple fluids, this approach is not monotonic as a function of temperature (Figs. 4 and 5).

(vi) The surface tensions calculated  $\gamma$  from the present theories are larger than those obtained in Ref. [10] and the temperature dependence is not as linear (Fig. 6).

(vii) All theories for the RPM find that for  $T/T_c \approx 0.6$  the scaled surface tension  $\tilde{\gamma} = \gamma^*/T_c^*$  is considerably smaller than the corresponding ratio for simple atomic liquids. We surmise that this is a genuine feature of ionic fluids.

Certain aspects of our theory warrant further discussion. The basis of our approach is the approximation for the inhomogeneous pair distribution function  $g_{ij}(\mathbf{r}, \mathbf{r}', \{\rho_i(\mathbf{r})\}, \alpha)$ , which is the key input for the theory. This has two intriguing consequences for the asymptotics of the correlation functions generated from the density functional. The first concerns the low-density behavior of the second moment correlation length  $\xi$ , referred to above. That the MSA and MSA1 do not yield the exact limiting behavior for  $\xi$  reflects the fact that even at low densities our approximation for  $g_{ij}$  does not capture the proper long-wavelength variation, i.e., the correct coefficient of  $k^2$  in the structure factor [Eq. (18)]. A possible improvement upon the present approximation for  $g_{ij}(\mathbf{r}, \mathbf{r}', \{\rho_i(\mathbf{r})\}, \alpha)$  may be given by the ‘‘mean density approximation’’ used in Refs. [34] and [41] in which the inhomogeneous pair distribution function is expanded around its homogeneous limit up to second order in the deviation  $\rho(\mathbf{r}) - \rho_b$ . However, as for DFTs based on a density expan-

sion of the excess free energy, this approach cannot be applied straightforwardly to the liquid-vapor interface due to the lack of a unique bulk density that could serve as a starting point for the expansion. The second intriguing consequence is that the MSA, through its integration over  $\alpha$  in function space [Eq. (4)], yields algebraically decaying bulk correlation functions and liquid-vapor density profiles, whereas the correct ultimate decay should be exponential in both cases. Once again this failure must be attributed to the simple approximation employed for the inhomogeneous pair correlation function. However, it is not clear what modifications to the theory should be introduced (other than simply omitting the  $\alpha$  integration as was done in the MSA1) in order to eliminate this feature.

We should also emphasize that the present DFT of the liquid-vapor interface is a mean-field treatment in that it does not incorporate the effects of either bulk critical fluctuations or interfacial capillary-wave-like fluctuations. In keeping with treatments of simple atomic fluids we argue that the density profiles and surface tensions we calculate from our theory are those of the bare or *intrinsic* interface. In order to estimate the additional broadening of the density profile arising from the interfacial fluctuations one could perform the standard Gaussian unfreezing of these fluctuations on the intrinsic interface given by the present theory [42,38]. The ‘‘stiffness’’ of the interface is determined by the dimensionless ratio  $\omega = k_B T / 4\pi \gamma \xi^2$ , i.e., the larger the surface tension  $\gamma$ , the smaller the interfacial broadening. Since we predict that in the RPM the ratio  $\tilde{\gamma} = \gamma a^2 / k_B T$  is much smaller than for an atomic fluid at the same reduced temperature  $T/T_c$ , this implies that the broadening due to fluctuations is significantly more pronounced for the RPM.

There are two other interesting problems to which the present theory could be applied. The first is the interface between an ionic fluid and a charged wall. Although this has been investigated using several theoretical techniques [21,19] the advantage of the present approach is that it incorporates two coexisting phases and thus can describe wetting phenomena. The second is the liquid-vapor interface of an ionic fluid in which cations and anions have unequal diameters. These more realistic systems have only been tackled within the context of the gradient expansion [43]. In both cases electrical double layers will form, giving a local violation of electroneutrality. However, the bulk correlation functions used as input to the DFT are only available for neutral systems. Nevertheless, one might still hope to capture the essential features by employing Eq. (5) for the mapping to the bulk system and by taking account of the nonzero local charge density only via the Coulomb contribution to the free energy, Eq. (6). A similar assumption has proved successful for the electrolyte-wall interface in the density-functional theories of Refs. [15–18].

## ACKNOWLEDGMENTS

We thank B. Götzemann and R.J.F. Leote de Carvalho for helpful discussions. R.E. is grateful for the hospitality of the physics department of the University of Wuppertal.

- [1] M. Parrinello and M.P. Tosi, Riv. Nuovo Cimento **2**, 1 (1979).
- [2] M.E. Fisher, J. Stat. Phys. **75**, 1 (1994); G. Stell, *ibid.* **78**, 197 (1995).
- [3] M.E. Fisher, J. Phys.: Condens. Matter **8**, 9103 (1996); G. Stell, *ibid.* **8**, 9329 (1996).
- [4] For a recent summary of experimental work see W. Schröer, M. Kleemeier, M. Plikat, V. Weiss, and S. Wiegand, J. Phys.: Condens. Matter **8**, 9321 (1996); an earlier review is given by J.M.H. Levelt Sengers and J.A. Given, Mol. Phys. **80**, 899 (1993).
- [5] R.J.F. Leote de Carvalho and R. Evans, J. Phys.: Condens. Matter **7**, L575 (1995).
- [6] M.E. Fisher and B.P. Lee, Phys. Rev. Lett. **77**, 3561 (1996).
- [7] J.M. Caillhol, D. Levesque, and J.J. Weis, J. Chem. Phys. **107**, 1565 (1997).
- [8] J.S. Rowlinson and B. Widom, *Molecular Theory of Capillarity* (Clarendon, Oxford, 1982).
- [9] D.M. Heyes and J.H.R. Clarke, J. Chem. Soc., Faraday Trans. 2 **75**, 1240 (1979).
- [10] M.M. Telo da Gama, R. Evans, and T.J. Sluckin, Mol. Phys. **41**, 1355 (1980).
- [11] R. Evans and T.J. Sluckin, Mol. Phys. **40**, 413 (1980).
- [12] J.S. Høye, J.L. Lebowitz, and G. Stell, J. Chem. Phys. **61**, 3253 (1974).
- [13] E. Waisman and J.L. Lebowitz, J. Chem. Phys. **56**, 3086 (1972).
- [14] E. Waisman and J.L. Lebowitz, J. Chem. Phys. **56**, 3093 (1972).
- [15] L. Mier-y-Teran, S.H. Suh, H.S. White, and H.T. Davis, J. Chem. Phys. **92**, 5087 (1990); Z. Tang, L. Mier-y-Teran, H.T. Davis, L.E. Scriven, and H.S. White, Mol. Phys. **71**, 369 (1990).
- [16] R.D. Groot, Phys. Rev. A **37**, 3456 (1988); R.D. Groot and J.P. van der Eerden, *ibid.* **38**, 296 (1988).
- [17] E. Kierlik and M.L. Rosinberg, Phys. Rev. A **44**, 5025 (1991).
- [18] C.N. Patra and S.K. Ghosh, Phys. Rev. E **47**, 4088 (1993); **48**, 1154 (1993).
- [19] P. Attard, Adv. Chem. Phys. **92**, 1 (1996).
- [20] R. Evans, P. Tarazona, and U. Marini Bettolo Marconi, Mol. Phys. **50**, 993 (1983).
- [21] L. Blum and D. Henderson, in *Fundamentals of Inhomogeneous Fluids*, edited by D. Henderson (Dekker, New York, 1992), p. 239.
- [22] R.F. Kayser, J. Phys. (France) **49**, 1027 (1988); Kinam **A8**, 87 (1987).
- [23] H. Tostmann, D. Nattland, and W. Freyland, J. Chem. Phys. **104**, 8777 (1996); S.C. Müller, H. Tostmann, D. Nattland, and W. Freyland, Ber. Bunsenges. Phys. Chem. **98**, 395 (1994).
- [24] R. Evans, Adv. Phys. **28**, 143 (1979).
- [25] S. Sokolowski and J. Fischer, J. Chem. Phys. **96**, 5441 (1992).
- [26] N.F. Carnahan and K.E. Starling, J. Chem. Phys. **51**, 635 (1969).
- [27] R. Evans, J.R. Henderson, D.C. Hoyle, A.O. Parry, and Z.A. Sabeur, Mol. Phys. **80**, 755 (1993).
- [28] R.J.F. Leote de Carvalho and R. Evans, Mol. Phys. **83**, 619 (1994).
- [29] D. Henderson and W.R. Smith, J. Stat. Phys. **19**, 191 (1978).
- [30] B. Guillot and Y. Guissani, Mol. Phys. **87**, 37 (1996).
- [31] Y. Levin and M.E. Fisher, Physica A **225**, 164 (1996).
- [32] G. Orkoulas and A.Z. Panagiotopoulos, J. Chem. Phys. **101**, 1452 (1994).
- [33] B. Smit, E. Esselink, and D. Frenkel, Mol. Phys. **87**, 159 (1996).
- [34] R. Evans and W. Schirmacher, J. Phys. C **11**, 2437 (1978).
- [35] B.P. Lee and M.E. Fisher, Phys. Rev. Lett. **76**, 2906 (1996). Note that in Eq. (13) of this reference the first part should read  $\xi_{GMSA} \approx (ab/8)^{1/2}$  and in the following sentence replace  $\xi_{GMSA}$  by  $\xi_{\infty, GMSA}$ .
- [36] J. Ennis, R. Kjellander, and D.J. Mitchell, J. Chem. Phys. **102**, 975 (1995).
- [37] P. Attard, Phys. Rev. E **48**, 3604 (1993).
- [38] See, e.g., R. Evans, in *Liquids at Interfaces*, Proceedings of the Les Houches Summer School of Theoretical Physics, Session XLVIII, edited by J. Charvolin, J.F. Joanny, and J. Zinn-Justin (North-Holland, Amsterdam, 1990), p. 4.
- [39] P. Frodl and S. Dietrich, Phys. Rev. A **45**, 7330 (1992); Phys. Rev. E **48**, 3203 (1993); **48**, 3741 (1993).
- [40] B.Q. Lu, R. Evans, and M.M. Telo da Gama, Mol. Phys. **55**, 1319 (1985), and references therein.
- [41] R.L. Henderson and N.W. Ashcroft, Phys. Rev. A **13**, 859 (1976).
- [42] J.W. Weeks, J. Chem. Phys. **67**, 3106 (1977).
- [43] T.J. Sluckin, J. Chem. Soc., Faraday Trans. 2 **77**, 1029 (1981).